



DØ Note 4871-CONF
Version 1.6

Search for Single Top Quark Production Using Likelihood Discriminants at DØ in Run II

The DØ Collaboration
<http://www-d0.fnal.gov>
(Dated: July 20, 2005)

We present an improved search for single top quarks in two production modes, s -channel (tb) and t -channel (tqb). The search is performed in the electron+jets and muon+jets decay channels, with one or more b -tagged jets, on nearly 370 pb^{-1} of DØ Run II data collected between August 2002 and August 2004. Impact-parameter based b -quark tagging is used to select signal-like events. We use a likelihood discriminant method to separate signals from backgrounds. The resulting expected/observed 95% confidence level upper limits on the single top quark production cross sections are 3.3/5.0 pb (s -channel) and 4.3/4.4 pb (t -channel).

Preliminary Results for Summer 2005 Conferences

I. INTRODUCTION

The top quark was originally discovered in 1995, at the Run I Fermilab Tevatron $p\bar{p}$ Collider by the CDF and DØ collaborations [1]. It was observed in its $t\bar{t}$ production mode via the strong interaction ($q\bar{q} \rightarrow g \rightarrow t\bar{t}$). Within the Standard Model, another production mode via the electroweak interaction is possible. This mode is called single top quark production as only one top quark is produced with another b quark through the Wtb vertex. As a consequence, a measurement of the single top quark production cross section can be used to constrain the magnitude of the CKM matrix element V_{tb} and study the properties of the Wtb coupling. The two main Feynman diagrams for s - and t -channel single top quark production at the Tevatron Run II are given in Fig. 1.



FIG. 1: The dominant Feynman diagrams for single top quark production at the Tevatron $p\bar{p}$ Collider: s -channel, tb final state (left diagram) and t -channel, tqb final state (right diagram). In this note, we use the simplified notation tb and tqb which implicitly includes all possible charge conjugations.

Single top quark production has not yet been observed [2–6] and is more challenging than $t\bar{t}$ production due to smaller cross sections (2.86 pb, see Table I) and a much larger, less discriminable background. We present a new analysis of $\sim 370 \text{ pb}^{-1}$ of DØ Run II data using a likelihood discriminant method to separate signals and backgrounds and we derive 95% confidence level upper limits to the s - and t -channel single top quark production cross sections.

Production channel	Cross Section [pb]
tb (s -channel)	0.88 ± 0.14
tqb (t -channel)	1.98 ± 0.30

TABLE I: Next-to-leading order single top quark production cross sections at $\sqrt{s} = 1.96 \text{ TeV}$ for $m_{top} = 175 \text{ GeV}$ [7–9]. Systematics uncertainties include the uncertainty on the top quark mass.

II. SIGNAL SIGNATURE

The top quark is the heaviest known particle. Its large mass and small decay length confer it unique properties. It decays before hadronization can occur, and spin information is preserved in the decay products, which leads to angular correlations in the final state objects that are characteristic for this signal. This analysis focuses on the final state topology where the top quark decays into a b quark and a W boson, which subsequently decays leptonically ($W \rightarrow e\nu, \mu\nu$). The signal signature consists of an isolated high transverse momentum lepton (electron or muon), significant missing transverse energy carried out by the neutrino and two or three high transverse momentum jets including at least one b jet. The largest backgrounds with a similar topology are the associated production of a W boson with jets (W +jets) and $t\bar{t}$ production. Additional multijet background comes from events containing a fake isolated lepton (jet identified as electron or muon from B hadron decays or decays in flight) associated with hadronic jets. Smaller contributions from diboson (WW, WZ) events are also considered.

III. THE DØ DETECTOR

The DØ detector for Run II, completely described in [10], consists of a central tracking system, a liquid-argon/uranium sampling calorimeter and an iron toroid muon spectrometer. The central tracking system is composed of a silicon microstrip tracker (SMT) and a central fiber tracker (CFT), both located into a 2T superconducting solenoidal magnet. The SMT detector has about 800000 individual strips and its design is optimized for tracking and

vertexing capabilities allowing heavy flavor tagging. The calorimeter is longitudinally segmented into electromagnetic and hadronic layers and is housed into three cryostats: a central barrel covering $|\eta| \lesssim 1.1$ and two end-caps that extend coverage up to $|\eta| \lesssim 4$. The muon system resides beyond the calorimeter and consists of a layer of tracking detectors and scintillation counters before the toroidal magnet, followed by two similar layers after the toroid. Tracking in the muon system relies on wide or mini drift tubes depending on the acceptance (up to $|\eta| = 2$).

IV. DATA AND SIMULATED SAMPLES

The analysis partitioned by decay mode, in electron and muon channels, is based on Run II data recorded between August 2002 and October 2004. The integrated luminosity is $366 \pm 24 \text{ pb}^{-1}$ for the electron channel and $363 \pm 24 \text{ pb}^{-1}$ for the muon channel. The different luminosities are due to different data quality requirements. The Monte Carlo samples for $t\bar{t} \rightarrow lvbj\bar{j}\bar{b}$ (lepton+jet), $t\bar{t} \rightarrow lvbl\nu\bar{b}$ (dileptons), W +jets (Wbb and Wjj) and diboson ($WW \rightarrow lvjj$, $WZ \rightarrow lvjj$) processes were generated using ALPGEN [11] for hard interaction matrix elements calculations (at leading order) coupled to PYTHIA [12] for initial state radiation, final state radiation, hadronization and fragmentation. Single top quark signal samples were produced with a modified version of COMHEP [13] interfaced to PYTHIA in order to reproduce the next-to-leading order kinematic distributions of the decay particles in the s -channel and t -channel. The Monte Carlo samples are processed with the full GEANT [14] simulation of the DØ detector and passed through the DØ event reconstruction program. The resulting lepton and jet energies are smeared to reproduce the resolutions observed in data.

V. EVENT RECONSTRUCTION AND SELECTION

The events are selected by requiring simple cuts on reconstructed objects. The event primary vertex must have at least 3 tracks and a position along the beam axis not greater than 60 cm from $z = 0$. Jets are reconstructed using the standard DØ cone algorithm (cone radius $\Delta R = \sqrt{(\Delta\eta)^2 + (\Delta\phi)^2} = 0.5$). For jets within the trigger system acceptance, we require that a corresponding energy deposition was observed in the Level 1 calorimeter system. Each event is required to have between two and four good jets with a leading jet satisfying $p_T > 25 \text{ GeV}$ and $|\eta| < 2.5$. Other good jets should have $p_T > 15 \text{ GeV}$ and $|\eta| < 3.4$. Jet energy is corrected for out-of-cone showering, calorimeter non uniformity, and the difference in calorimeter response between electrons and pions. Electrons are reconstructed using information from both the calorimeter and the central tracker. Muons are reconstructed using information from the muon spectrometer with a detector pseudorapidity acceptance $|\eta^{det}| < 2$. The event must contain only one isolated lepton with $p_T > 15 \text{ GeV}$. For the electron channel, only electrons in the central part of the calorimeter ($|\eta^{det}| < 1.1$) are considered. Both muon and electron must be well matched to a track. Muon candidates within a jet ($\Delta R(\mu, jet) < 0.5$) are rejected. In order to account for the presence of a neutrino, some constraints are applied on the missing transverse energy (\cancel{E}_T) (corrected for the presence of electrons, muons and jets in the event). We require $\cancel{E}_T^{JES} > 15 \text{ GeV}$ and $15 < \cancel{E}_T < 200 \text{ GeV}$, where \cancel{E}_T^{JES} is the missing transverse energy with jet energy scale correction applied and \cancel{E}_T has also corrections for the energy of an isolated muon. QCD multijet events, where \cancel{E}_T results from misreconstructed objects (jets or electrons), are rejected by imposing cuts in the planes $\cancel{E}_T - \Delta\phi(\text{lepton}, \cancel{E}_T)$ and $\cancel{E}_T - \Delta\phi(\text{jet}, \cancel{E}_T)$. Finally, at least one of the good jets must satisfy the Tight b -tagging criteria (see next Section).

VI. LIFETIME B-TAGGING

The event selection requires at least one b -tagged jet. Prior to tagging we require calorimeter jets to be taggable i.e. matched to a track jet. We are using the Jet Lifetime Probability (JLIP) algorithm of the DØ Collaboration [15]. It uses the signed impact parameter of tracks (representing the distance of closest approach of a track w.r.t the primary vertex) within a jet to compute a probability for the jet to originate from the primary vertex. Heavy quark jets are expected to have low values for the JLIP probability. Jets are tagged if their JLIP probability is smaller than a given cut. The probability distribution is expected to be flat for light jets and therefore the cut value gives approximately the mistag rate. In this analysis we are using two different probability cuts: Tight ($P_{JLIP} < 0.3\%$) and Loose ($P_{JLIP} < 1.0\%$). Efficiencies (including taggability) for each probability cuts are given in Fig. 2. The dataset is split into two orthogonal tagging schemes. The “single tag” sample corresponds to events containing exactly one Tight and no extra Loose b -tagged jet. The “double tag” sample is associated to events with at least one Tight and another Loose b -tagged jets.

VII. YIELDS FOR SIGNALS AND BACKGROUNDS

The analysis follows the same strategy as in Ref. [6]. The general selection described in section V is designed to reject misreconstructed events and to select a signal-like data sample that is well reproduced by Monte Carlo

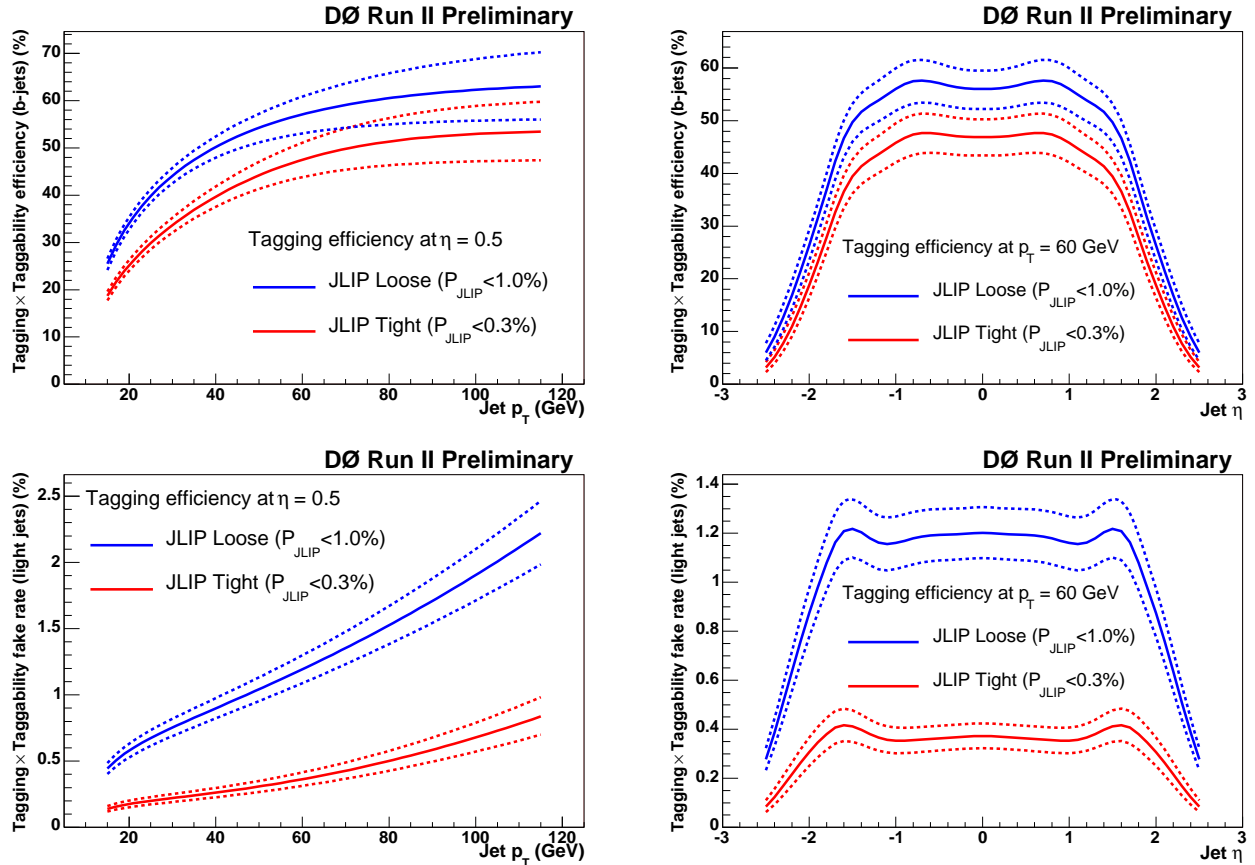


FIG. 2: JLIP b -tagging efficiencies in the electron channel data as a function of jet p_T (at $\eta = 0.5$) and jet η (at $p_T = 60$ GeV) for the Loose (red curve) and Tight (blue curve) probability cuts. These curves include the taggability efficiency. The first row corresponds to the b -jets tagging efficiency and the second to the light jet mistag rate. The dashed curves correspond to the total $\pm 1\sigma$ systematic error bands.

backgrounds samples. The b -tagging requirement enhances the discrimination between signals and the W +light jet and multijet backgrounds. We estimate, mostly from Monte Carlo samples, the yields for the main backgrounds after the final procedure which includes trigger and selection effects as well as b -quark jet tagging. Different normalization procedures are applied for the processes considered in this analysis. The numbers of selected data events before tagging containing a fake (N_{fake}) or a real (N_{real}) isolated lepton is used to normalize the W +jets and QCD multijet backgrounds. The electron quality requirements (based on a multivariate likelihood) and the muon isolation criteria are described in [16].

- The multijet background yield is estimated from data by applying the selection and b -tagging but reversing the lepton isolation criteria. The number of selected events before tagging is normalized to N_{fake} .
- The W +jets background yield is derived from Wjj (including Wcc) and Wbb Monte Carlo samples. The total number of W +jets background events before tagging is normalized to N_{real} . The relative contribution of Wbb to Wjj is provided by the ratio of corresponding theoretical cross sections. Finally, each W +jets Monte Carlo event is weighted by its b -tagging probability.
- Single top quark, top quark pair and diboson yields are fully estimated using Monte Carlo samples. Selection cuts are applied. Events are weighted by their probability to pass the trigger and b -tagging requirements. Correction factors describing selection efficiency differences between data and Monte Carlo are also applied. The final normalization is made using the theoretical cross sections and the measured luminosity.

Yields for signals and background are summed up in Table II.

	Signals and backgrounds yields with uncertainties			
	Electron channel		Muon channel	
	Single tag	Double tag	Single tag	Double tag
Signals yields				
$t\bar{b}$	3.3 ± 0.5	1.6 ± 0.4	3.0 ± 0.5	1.6 ± 0.4
$tq\bar{b}$	6.9 ± 1.3	1.0 ± 0.2	6.2 ± 1.3	0.9 ± 0.2
Backgrounds yields				
$t\bar{t} \rightarrow \text{lepton} + \text{jets}$	40.4 ± 8.9	20.3 ± 5.4	37.6 ± 8.4	20.6 ± 5.7
$t\bar{t} \rightarrow \text{dilepton}$	11.3 ± 2.5	5.5 ± 1.5	10.2 ± 2.3	5.2 ± 1.5
Wbb	24.2 ± 1.6	8.1 ± 1.6	14.7 ± 1.0	5.4 ± 1.2
Wjj	111.6 ± 11.0	4.9 ± 1.1	74.7 ± 7.8	3.4 ± 0.8
WW	2.3 ± 0.5	< 0.1	2.4 ± 0.6	< 0.1
WZ	2.0 ± 0.5	0.7 ± 0.2	1.8 ± 0.4	0.7 ± 0.7
Multijet	21.8 ± 3.7	1.4 ± 0.3	17.9 ± 4.5	2.7 ± 0.4
Total backgrounds	213.6 ± 20.7	40.9 ± 8.5	159.3 ± 17.6	38.0 ± 8.4
Data yield with stat. uncertainties	229 ± 15.1	43 ± 6.6	138 ± 11.7	33 ± 5.7

TABLE II: Signal and background yields with total uncertainties.

VIII. LIKELIHOOD DISCRIMINANT METHOD

After the event selection, a final discriminating variable is constructed in order to efficiently characterize the signal type events and reject the background type ones. This likelihood variable is a robust statistical variable and is a more efficient way of separating signal from background than sequential cuts since a likelihood uses the entire shape of the signal and background distributions to distinguish between them. The use of a likelihood method is adequate as the sample size is reasonable and the distributions consist of essentially uncorrelated variables.

The final discriminating variable is achieved by using a vector of measurements \vec{x} , on the basis of the single quality $\mathcal{L}(\vec{x})$:

$$\mathcal{L}(\vec{x}) = \frac{\mathcal{P}_{\text{signal}}(\vec{x})}{\mathcal{P}_{\text{signal}}(\vec{x}) + \mathcal{P}_{\text{background}}(\vec{x})}$$

where $\mathcal{P}_{\text{signal}}(\vec{x})$ and $\mathcal{P}_{\text{background}}(\vec{x})$ are the probability density functions for two categories of events. The optimal event-classification scheme selects events having the largest values for the ratio of probabilities $\mathcal{P}_{\text{signal}}(\vec{x})/\mathcal{P}_{\text{background}}(\vec{x})$ to define a sample enriched in signal events. Signal events tend to have a value of \mathcal{L} close to 1, whereas background events have a value near 0.

The probability density functions $\mathcal{P}_{\text{signal}}(\vec{x})$ and $\mathcal{P}_{\text{background}}(\vec{x})$ are determined from the product of Monte Carlo one dimensional distributions of the input variables, therefore potential correlations between variables are not taken into account.

As the main backgrounds ($t\bar{t}$ production and W +jets) have different topologies, we choose to build two likelihood discriminants for each channel: a signal/ $t\bar{t}$ filter and a signal/ W +jets filter. Electron and muon channels in each tagging scheme are treated as independent channels, and are combined in the limit calculation, which leads to a total of 16 likelihood discriminant variables.

Many sets of variables were tested to build the likelihood discriminants, including transverse momenta, invariant masses and angular variables combining the different reconstructed objects (lepton, neutrino, jets). The final set of variables was selected to optimize the discrimination of the likelihood variables. We finally retain the following variables to construct the discriminating likelihood variables. Table III summarizes the variables used for each category of filter:

- The transverse momentum of the leading jet, $p_T(\text{jet1})$.
- The transverse momentum of the second leading jet, $p_T(\text{jet2})$.
- The transverse momentum of the third leading jet if it exists, $p_T(\text{jet3})$.
- The scalar sum of the missing transverse energy and the transverse energy of the lepton, METLep.
- The invariant mass of the system of all jets, i.e. the four-vector sum of all jets in the events, M_{alljets} .

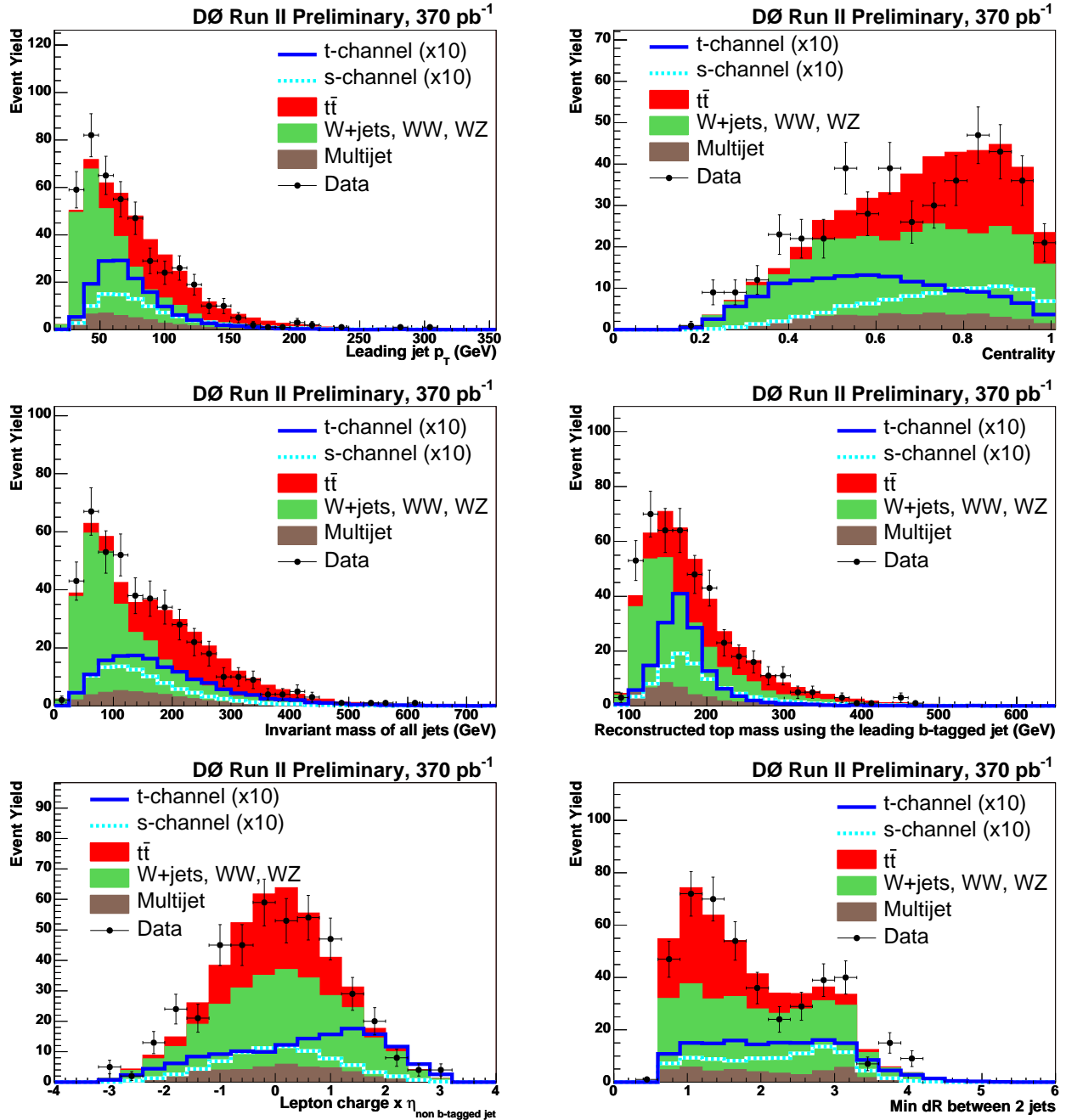


FIG. 3: Electron and muon channels combined. Distributions of the $p_T(\text{jet}1)$, Centrality, M_{alljets} , $M(W, \text{tagjet}1)$, $Q \times \eta$ and $\Delta R_{\text{min}}(\text{alljets})$ variables (see text for definitions) for combined single and double tags. Signal distributions (blue curves) are scaled by a factor 10 for better legibility.

- The transverse mass of the W boson.

$$M_T(W) = \sqrt{(p_T^{\text{lepton}} + \cancel{E}_T)^2 - (p_x^{\text{lepton}} + \cancel{E}_{Tx})^2 - (p_y^{\text{lepton}} + \cancel{E}_{Ty})^2}.$$
 This variable is mostly used to reject multi-jet background events.

- The invariant mass of the system of the W boson (i.e. Lorentz vector of the neutrino and the lepton) and the leading tagged jet $M(W, \text{tagjet}1)$. This variable corresponds to the reconstructed top quark mass. The transverse component of the neutrino momentum is reconstructed from the missing transverse energy in the event. The z component of the neutrino momentum is obtained from a W boson mass constraint, choosing the smaller $|p_z(\nu)|$ solution of the two possible solutions. When the two solutions have complex values, the real part of the complex value is chosen. This procedure identifies the correct $p_z(\nu)$ in about 70% of the events.

- The minimum angular separation $\Delta R = \sqrt{\phi^2 + \eta^2}$ between all the jets, $\Delta R_{min}(\text{alljets})$.
- The cosine of the angle between the second leading jet and the lepton in the top rest frame, $\cos(\text{jet2}, \text{lepton})_{\text{top}}$.
- The sphericity of the event, $\mathcal{S} = \frac{3}{2}(\lambda_2 + \lambda_3)$, where λ_2 and λ_3 are the smallest eigenvalues of the normalized momentum tensor $\mathcal{M}_{ij} = \frac{\sum_{jets} p_i \cdot p_j}{\sum_{jets} |\mathbf{p}|^2}$.
- The centrality of the event, $\mathcal{C} = \frac{\sum_{jets} p_T}{\sum_{jets} |\mathbf{p}|}$.
- The $Q \times \eta$ variable which is the charge of the lepton, multiplied by the pseudorapidity of the leading untagged jet. In the t -channel, the final state d quark produced with the top quark tends to go along the incoming proton direction. Similarly, the \bar{d} quark produced with the anti-top quark goes along the anti-proton direction. We take this CP symmetry into account through multiplying the η distribution by the charge of the lepton, which reflects the charge of the top quark.

	$tb/W+\text{jets}$	$tb/t\bar{t}$	$tqb/W+\text{jets}$	$tqb/t\bar{t}$
1. $p_T(\text{jet1})$	✓	✓	✓	✓
2. $p_T(\text{jet2})$	✓	✓	✓	✓
3. $p_T(\text{jet3})$	—	✓	—	✓
4. METLep	✓	✓	✓	✓
5. M_{alljets}	✓	✓	✓	✓
6. $M_T(W)$	✓	✓	✓	✓
7. $M(W, \text{tagjet1})$	✓	—	✓	—
8. $\Delta R_{min}(\text{alljets})$	—	✓	—	✓
9. $\cos(\text{jet2}, \text{lepton})_{\text{top}}$	✓	—	✓	—
10. Sphericity	—	✓	—	✓
11. Centrality	—	✓	—	✓
12. $Q \times \eta$	—	—	✓	✓

TABLE III: Input variables used for each likelihood discriminant.

Some distributions of the previous variables are shown in Fig. 3 for combined electron and muon channels and combined single and double tags. Examples of likelihood filters outputs for signal and backgrounds are given in Fig. 4 and 5.

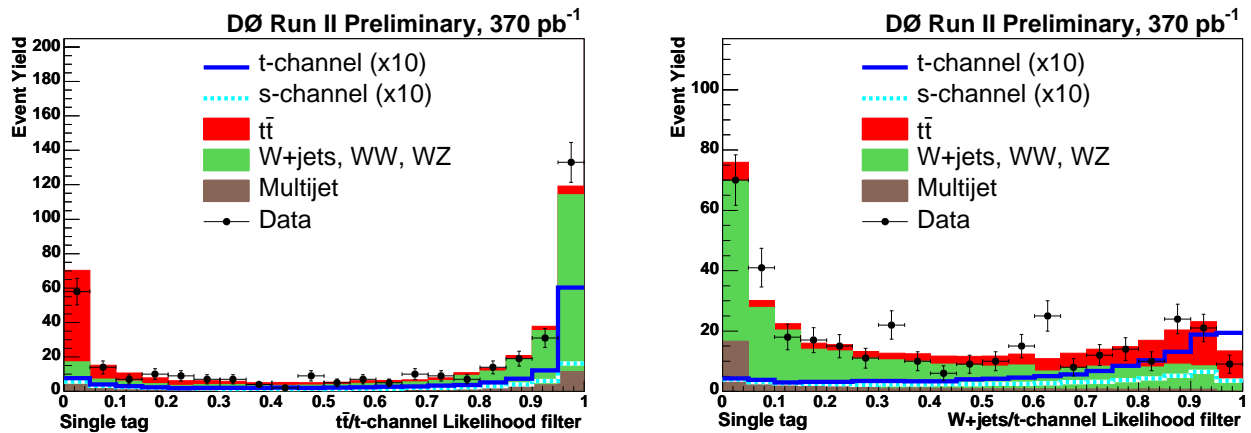


FIG. 4: Electron and muon channels combined. Data to Monte-Carlo comparison for the $tqb/t\bar{t}$ (left) and $tqb/W+\text{jets}$ (right) filters for single tagged events.

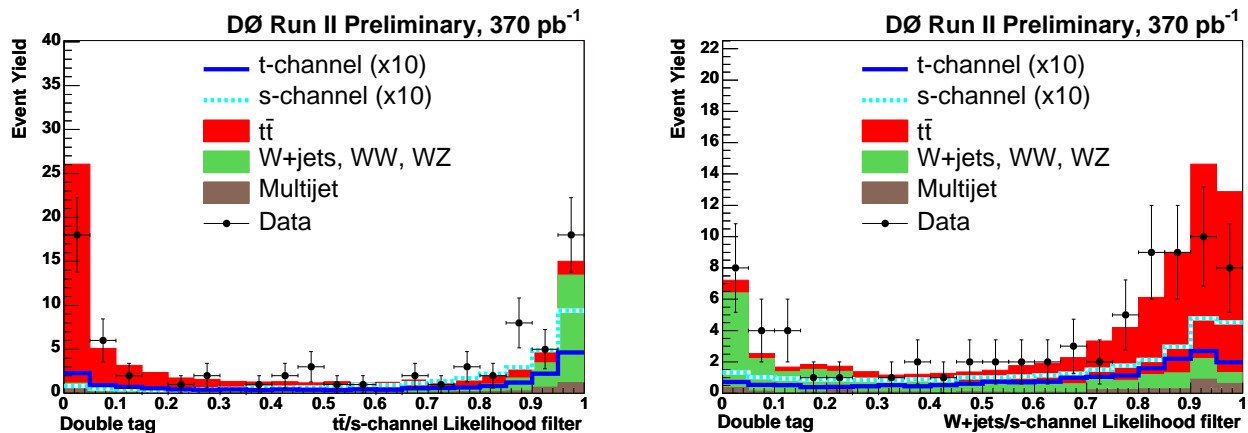


FIG. 5: Electron and muon channels combined. Data to Monte-Carlo comparison for the $tb/t\bar{t}$ (left) and tb/W +jets (right) filters for double tagged events.

IX. SYSTEMATIC UNCERTAINTIES

Systematic uncertainties on the yields are evaluated separately for electron and muon channels for each b -tagging scheme. Sources of systematics and their range values are summarized in Table IV for Monte Carlo yields ($t\bar{t}$, diboson) and in Table V for yields normalized to data (multijet and W +jets) [17].

Systematics uncertainties (%)	
Luminosity [17]	6.5
Cross section	2(WW)-18($t\bar{t}$)
Branching fraction	2
Primary vertex reconstruction	2
Electron identification	4
Muon identification	5
Jet identification	1-4
Jet energy scale	1-5
Jet energy resolution	1
Jet fragmentation	5
Trigger modeling	2-7
Single (double) b -tag modeling	6 (17)
Samples statistics	1

TABLE IV: Averaged systematic uncertainties for Monte Carlo estimated yields.

Systematics uncertainties (%)	
Data normalization	5-15
Single (double) b -tag modeling (W +jets only)	9 (15)
Samples statistics	3 (2-17)

TABLE V: Averaged systematic uncertainties for data normalized yields.

X. CROSS SECTION LIMITS

The number of observed events is consistent with the background prediction for both muon and electron channels and for all b -tagging schemes, within the total uncertainties. We therefore set upper limits at the 95% confidence level, using a Bayesian approach [18]. We use two-dimensional distributions of the signal/ W +jets likelihood discriminant vs. signal/ $t\bar{t}$ likelihood discriminant (see Fig 6). We assume a Poisson distribution for the observed counts, and a flat prior probability for the signal cross section. The priors for the signal acceptance and the backgrounds are multivariate Gaussians centered on their estimates and described by a covariance error matrix taking into account correlations across the different sources and bins. We combined the four orthogonal analysis channels (electron and muon, single and double tags) to enhance the sensitivity of the analysis. Plots for the Bayesian posterior density are provided in Fig 7. The observed (expected) 95 % confidence level limits are 5.0 pb (3.3 pb) for the s -channel and 4.4 pb (4.3 pb) for the t -channel. This result improves the previous limit published by the DØ Collaboration [6]. Both analyses have very similar strategies, the main differences being the b -tagging algorithm, the final discriminant and the integrated luminosity (see Table VI). Some systematics uncertainties were also reduced. In order to compare the sensitivity of

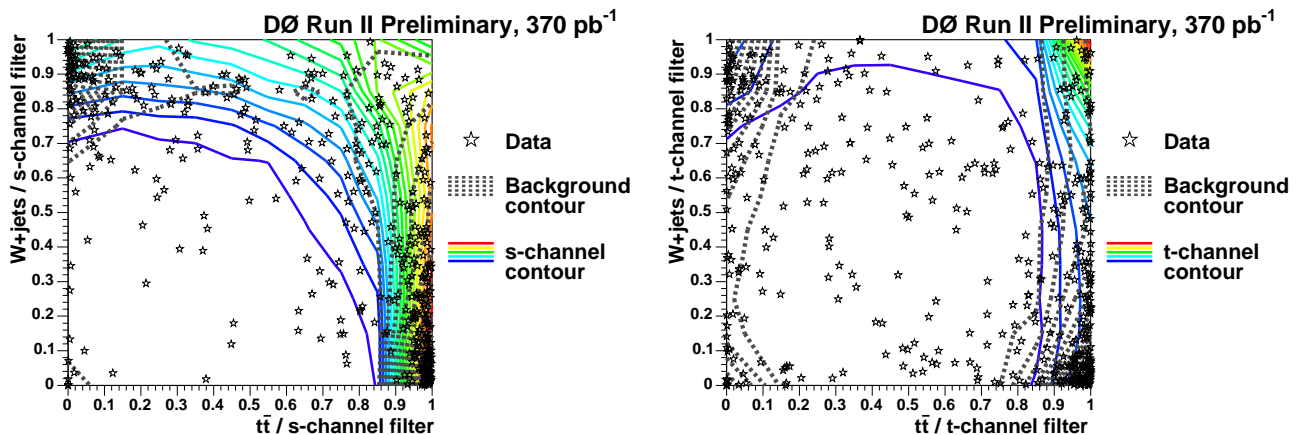


FIG. 6: Two-dimensional distributions of $W+\text{jet}$ filter vs. $t\bar{t}$ filter, comparing the total background estimate (dashed contour), signal estimate (plain gray contour), and observed data (stars) for s -channel (left) and t -channel (right) searches. Electron and muon channels, single and double tagged have been summed on these plots.

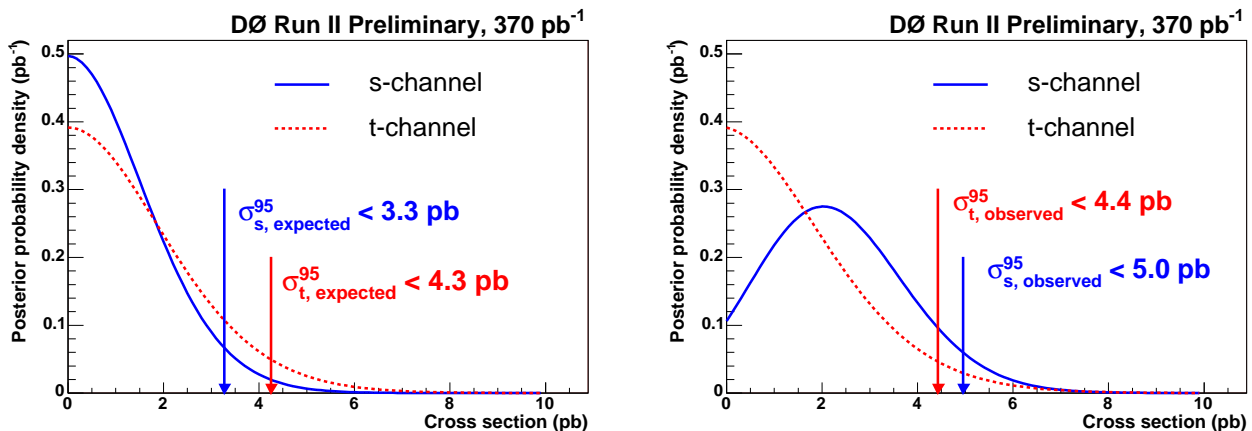


FIG. 7: Expected (left) and observed (right) Bayesian posterior densities with 95% confidence level limits for combined electron and muon channel and combined b -tagging schemes.

the two analysis, we rescaled the estimated yields and statistical errors to a luminosity of 230 pb^{-1} and recomputed the expected limits with and without systematic uncertainties (see Table VII). The sensitivities of both methods are very similar, even if the likelihood discriminant, opposed to the neural network, does not take correlations between variables into account. The gain on the final limits comes mostly from the increased luminosity.

	Analysis	
	Published [6]	Current
Luminosity	230 pb^{-1}	370 pb^{-1}
b -tagging algorithm	Secondary vertex (SVT)	Jet Lifetime Probability (JLIP)
Final discriminant method	Neural networks	Likelihood discriminant

TABLE VI: Main differences between the published $D\phi$ analysis [6] and the current result.

XI. SUMMARY

We analyzed nearly 370 pb^{-1} of data collected by the $D\phi$ Run II detector. Separate analyses in electron+jets and muon+jets final state, with one or two identified b -quark jets were combined to improve the sensitivity. Upper limits at the 95% confidence level on the cross section for each s - and t -channel production modes have been set using a Bayesian fit to likelihood discriminant distributions. The final limits of 5.0 pb for the s -channel and 4.4 pb for the

	<u>Analysis</u>			
	<i>s</i> -channel		<i>t</i> -channel	
	Published [6]	Current	Published [6]	Current
without systematics	3.6 pb	3.6 pb	4.6 pb	4.8 pb
with systematics	4.4 pb	4.1 pb	5.8 pb	5.5 pb

TABLE VII: Expected 95% confidence level limits for a luminosity of 230 pb^{-1} for the published $D\bar{O}$ analysis [6] and the current analysis (rescaled to the same luminosity).

t-channel represent significant improvements over previous limits [2–6]. Compared to the recent $D\bar{O}$ publication [6], this analysis uses a simpler final analysis method that still gives comparable sensitivity. With the sensitivity of the current analysis, several fb^{-1} of data would be needed for an observation of single top quark production.

Acknowledgments

We thank the staffs at Fermilab and collaborating institutions, and acknowledge support from the DOE and NSF (USA); CEA and CNRS/IN2P3 (France); FASI, Rosatom and RFBR (Russia); CAPES, CNPq, FAPERJ, FAPESP and FUNDUNESP (Brazil); DAE and DST (India); Colciencias (Colombia); CONACyT (Mexico); KRF (Korea); CONICET and UBACyT (Argentina); FOM (The Netherlands); PPARC (United Kingdom); MSMT (Czech Republic); CRC Program, CFI, NSERC and WestGrid Project (Canada); BMBF and DFG (Germany); SFI (Ireland); Research Corporation, Alexander von Humboldt Foundation, and the Marie Curie Program.

-
- [1] F. Abe *et al.*, (CDF Collaboration), “Observation of Top Quark Production in $p\bar{p}$ Collisions,” Phys. Rev. Lett. **74**, 2626 (1995); S. Abachi *et al.*, (DØ Collaboration), “Observation of the Top Quark,” Phys. Rev. Lett. **74**, 2632 (1995).
- [2] B. Abbott *et al.*, (DØ Collaboration), “Search for Electroweak Production of Single Top Quarks in $p\bar{p}$ Collisions,” Phys. Rev. D **63**, 031101 (2001).
- [3] V.M. Abazov *et al.*, (DØ Collaboration), “Search for Single Top Quark Production at DØ Using Neural Networks,” Phys. Lett. **B517**, 282 (2001).
- [4] D. Acosta *et al.*, (CDF Collaboration), “Search for Single Top Quark Production in $p\bar{p}$ Collisions at $\sqrt{s} = 1.8$ TeV,” Phys. Rev. D **65**, 091102 (2002).
- [5] D. Acosta *et al.*, (CDF Collaboration), “Search for Electroweak Single-Top-Quark Production in $p\bar{p}$ Collisions at $\sqrt{s} = 1.96$ TeV” Phys. Rev. D **71**, 012005 (2005),
- [6] V.M. Abazov *et al.*, (DØ Collaboration), “Search for single top quark production in pbarp collisions at sqrt(s)=1.96 TeV” hep-ex/0505063; Fermilab-Pub-05/207-E, to be published in Phys. Lett. B (2005).
- [7] B.W. Harris, E. Laenen, L. Phaf, Z. Sullivan, and S. Weinzierl, “Fully Differential Single-Top-Quark Cross Section in Next-to-Leading Order QCD,” Phys. Rev. D **66**, 054024 (2002); Z. Sullivan, “Understanding Single-Top-Quark Production and Jets at Hadron Colliders,” to appear in Phys. Rev. D, hep-ph/0408049.
- [8] J. Campbell, R. K. Ellis and F. Tramontano, “Single Top Production and Decay at Next-to-Leading Order,” Phys. Rev. D **70**, 094012 (2004).
- [9] Q.-H. Cao, R. Schwienhorst, and C.-P. Yuan, “Next-to-Leading Order Corrections to Single Top Quark Production and Decay at the Tevatron: 1: s-channel process,” to appear in Phys. Rev. D, hep-ph/0409040 (2004).
- [10] V. Abazov *et al.*, DØ Collaboration, in preparation for submission to Nucl. Instrum. Methods in Phys. Res. **A**; T. LeCompte and H.T. Diehl, Ann. Rev. Nucl. Part. Sci. **50**, 71 (2000).
- [11] M.L. Mangano, M. Moretti, F. Piccinini, R. Pittau, and A.D. Polosa, “ALPGEN v1.3, a Generator for Hard Multiparton Processes in Hadronic Collisions,” J. High Energy Physics **0307**, 001 (2003).
- [12] T. Sjöstrand *et al.*, “PYTHIA 6.2: Physics and Manual,” hep-ph/0108264.
- [13] E. Boos *et al.*, (CompHEP Collaboration), “CompHEP 4.4: Automatic Computations from Lagrangians to Events,” Nucl. Instrum. Meth. A **534**, 250 (2004);
E.E. Boos, L.V. Dudko, and V.I. Savrin, “‘SingleTop’ — an Event Generator for the Single Top Quark Production at the LHC,” CMSNote 2000/065.
- [14] R. Brun *et al.*, “GEANT - Detector Description and Simulation,” CERN Program Library Long Writeup W 5013 (1994).
- [15] S. Greder, Ph.D. thesis, Université Louis Pasteur, Strasbourg, IRES 05-006 N° d’ordre ULP 4652 (2005).
- [16] V.M. Abazov *et al.*, (DØ Collaboration), hep-ex/0504043.
- [17] T. Edwards *et al.* (DØ Collaboration), “Determination of the Effective Inelastic $p\bar{p}$ Cross-Section for the DØ Run II Luminosity Measurement,” FERMLAB-TM-2278-E (2004).
- [18] I. Bertram *et al.*, “A Recipe for the Construction of Confidence Limits,” Fermilab-TM-2104 (2000).